〈일반논문〉
Journal of the Korean Society of Visualization, Vol. 17, No. 2 (90~95), 2019
(Manuscript received : 2019.08.07./Revised : 2019.08.27./Accepted : 2019.08.28.)
DOI:http://dx.doi.org/10.5407/jksv.2019.17.2.090

ISSN 1598-8430 Print
ISSN 2093-808X Online

유체 렌즈의 초점과 유동 인자의 상관관계에 대한 수치해석

Mohsen Lahooti · 김대겸†

Numerical study on the relation between flow parameters and the focal point of fluidic lens

Mohsen Lahooti and Daegyoum Kim†

Abstract In the present work, the effect of flow parameters such as volume flow rate on focal point of fluidic micro lens is investigated numerically. ANSYS Fluent is used for simulations, and the flow parameters and number of simulations are determined using the space filling method of design of experiment (DOE). Having determined the location of interfaces between fluids inside the micro lens which acts as the lens curvature, a ray tracking simulation on each case is performed using COMSOL Multiphysics to determine the focal point for each lens. These data are then used to provide a relation between flow parameters and the focal point of the lens.

Key Words : fluidic lens, immiscible fluids, focal point, ray tracking

1. Introduction

Optical lenses are widely used in many areas, including photography, medical and health industries, renewable energy production and astronomy. However, traditionally, such lenses are produced with a specific curvature and without flexibility, which confined their usage to the specific design criteria due to their fixed focal point. In order to change the focal point, it is customary to use more than one lens to provide a variable focal point. On the other hand, the micro device technology provides a reliable solution to overcome this shortcoming of traditional lenses via micro optofluidic lenses. Micro optofluidic lenses are devices in micro scale that consist of two or more immiscible fluids, for which their multiphase flow provide an interface. This interface acts as the lens curvature and by changing the curvature we are able to change the convergence and focal point of the lens [1,2]. Micro optofluidic lenses have different types and shapes including L-Grin hydro lenses [3] with two streams of flow and four passages to guide the flow motion, multi-convex curved duct hydro lenses [4] and air-liquid micro lenses [2,5] to name a few.

There are several researches reported in literature investigating various designs of micro lenses. Dong and Jiang studied the effects of pH on the surface curvature between two fluids and its effect on

† Department of Mechanical Engineeing, KAIST 34141, Daejeon, Republic of Korea
E-mail: daegyoum@kaist.ac.kr

focal length in micro bubble lenses. [6]. They showed that increasing the concentration of water will at first result in the increase in the focal length, while a further increase in concentration reduces the focal point. Dong and Agarwal investigated the effect of air pressure on the micro curvature of a bubble lens and concluded that the increase in pressure increased the curvature and hence decreased the focal point of the device [7]. Tang et. al. [8] investigated the effect of material of the micro lens itself. Mao et. al. [9] designed a micro L-GRIN lens with two flow streams with adjustable focal point and ability to scatter the light. Furthermore, Mao et. al. [10] investigated the effect of flow rates on the focal points of cylindrical micro-lens. There are numerous literature on the adjustable micro lenses which use various methods such as pneumatic control [11], manipulating refractive index via temperature and concentration [12] or utilizing electric field [1] and electrowetting [13]. However, there are few works that numerically studied the subject or provides the relation between flow rates and focal point for the plane two fluids micro lenses [14,15]. This motivated us to investigate numerically the effect of volume flow rate on focal point of a plane rectangular micro lens and provide a relation between the flow rate and focal points.

The rest of the paper is organized as follows: Sec. 2 introduces problem definition and numerical method, in Sec. 3, results and discussion are provided, and finally in Sec. 4 we conclude our work.

2. Problem description

2.1 Micro lens model

The micro lens considered in this work is a square domain with the length of 900 μm with five inlets on the left side and two outlets on the right side as shown in Fig. 1. The width of all ducts attached to the main domain is 50 μm. The micro lens consists of five streams of three immiscible fluids. The main fluid (core flow) flows with volume flow rate of Q_0 at the center and two auxiliary flows to help producing the desired curvature (Fig. 1). Auxiliary fluid 2 (here after AF1 for simplicity) enters the domain from top and bottom with the angle of 45° with volume flow rates of Q_3 while auxiliary fluid 2 (AF2 for simplicity) is injected parallel to core flow and has different volume flow rates at top and bottom (Fig. 1).

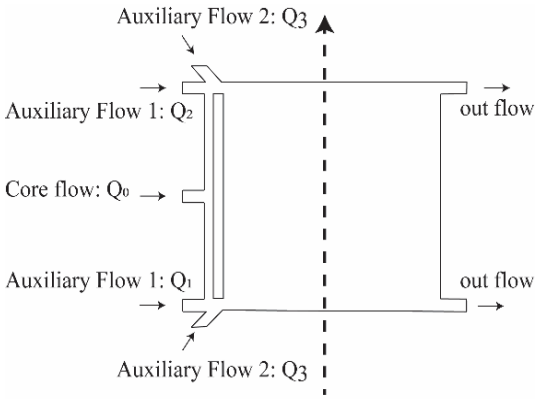

Fig. 1. Schematic of the micro lens. The dashed arrow shows the direction of a light ray

To provide flexibility on refraction indices, five different fluids with different refraction indices are considered and used in two general cases. In case A, Ethanol, cynnemaldehyde and mixture of 73.5% Ethylene glycol and 26.5% Ethanol that for simplicity we refer to it as the “mixture” are used for the core, AF1 and AF2 respectively. In case B Ionized water, Benzyl alcohol and mixture are used for core, AF1 and AF2 respectively. Table 1 summarizes the fluids and their properties used in our simulations.

To determine a relation between flow rates into the micro lens and the focal point of the lens, we consider the flow Reynolds number in range of 1-30

Table 1. Summary of fluids in micro lens with their thermophysical and optical properties

fluid	Density (kg/m^3)	Viscosity (mPa·s)	Refraction index (n)
Ethanol	789	1.04	1.36
Benzyl alcohol	1044	8	1.54
Ionized water	997	0.89	1.33
Cinnamaldehyde	1050	5.7	1.62
Silicone oil	868	0.65	1.38
Mixture of 73.5% Ethylene glycol and 26.5% Ethanol	915	9.8	1.41

which corresponds to the working range of these devices [2,3]. Furthermore, because there are five flow streams of three immiscible fluids to the micro lens, we used the following assumptions in order to reduce our variable spaces. First of all the AF2 is injected to the domain from top and bottom (Fig. 1) with the same volume flow rate: Q_3. For AF1 we considered two different volume flow rates, Q_1 and Q_2 at the bottom and top of the micro lens respectively. These different flow rates for AF2 result in a more flexible control on the focal point of the device. Additionally, in all simulations, the ratio of volume flow rate for AF2 to Q_1 is always kept constant: $q_1^* = Q_3/Q_1 = 0.1$; all other volume flow rates are also non-dimensionalized with Q_1. Using these constraints, the JMP® SAS software is used with the space filling method to determine the number of simulations and their corresponding conditions for case A and B. For each case, the DOE design suggested fifty simulations that can provide required data for the final regression between volume flow rates and focal points.

2.2 Numerical method

The fluid flow simulations are performed using ANSYS Fluent, where SIMPLE algorithm is used for velocity-pressure coupling and the multi-phase flow is handled via VOF method. Velocity inlet and pressure outlet are used for inflow and outflow boundaries respectively. For grid study, we simulate five cases with 0.6×10^5, 1.2×10^5, 2.4×10^5, and 4.8×10^5 cells, and results showed the convergence with 2.4×10^5 grid cells with less than 0.1% error to the finer mesh. After each simulation, the location of the interface is determined for the volume fraction of ϕ = 0.5 and exported for the subsequent analysis of ray tracking. The ray tracking is performed with the ray optic module of COMSOL Multiphysics. For ray tracking, COMSOL numerically solves the following system of equations:

$$\frac{\partial \mathbf{q}}{\partial t} = \frac{\partial \omega(\mathbf{K})}{\partial \mathbf{K}} \tag{1}$$

$$\frac{\partial \mathbf{K}}{\partial t} = -\frac{\partial \omega(\mathbf{K})}{\partial \mathbf{q}} \tag{2}$$

where $\mathbf{q}$ and $\mathbf{K}$ are ray position and wave vectors and ω is angular frequency. For the homogeneous medium, without gradient of refractive index, Eqs. (1) and (2) are reduced to

$$\frac{\partial \mathbf{q}}{\partial t} = \frac{c\mathbf{K}}{n|\mathbf{K}|} \tag{3}$$

$$\frac{\partial \mathbf{K}}{\partial t} = 0 \tag{4}$$

where n is the refractive index and c is the speed of light in vacuum. In the case of heterogeneous medium where a discontinuity occurs at the refractive indices such as interfaces, the new direction of the ray is computed numerically using Snell's law:

$$\frac{\sin\theta_2}{\sin\theta_1} = \frac{n_1}{n_2} \tag{5}$$

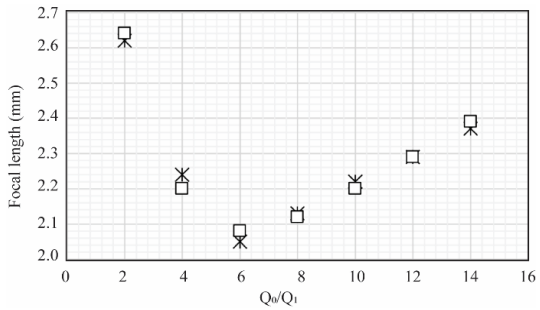

Fig. 2. Comparison of present results (square markers) with experimental measurements (star markers) [3].

To validate our simulations, we compare our results on the focal point of micro lens with the experimental measurements reported in [3]. Fig. 2 shows excellent agreement between the focal points computed (squares) with the one reported in [3] (stars) for various flow rates.

3. Results and discussion

3.1 Flow field and the shape of fluidic lens

Fig. 3 shows the interface location via contours of volume fraction of AF1 for two different simulations from case A and case B. Fig. 3(a) corresponds to simulation with Re = 1 with q_0* = 1.5 and q_2* = 0.6 while Fig. 3(b) is for Re = 30 with q_0* = 8.8 and q_2* = 2.0. These two sample simulations are selected to emphasize different configurations in the interface occurring in micro lens for various Reynolds numbers and flow rates. As evident in the figure, increasing the core Re confines the penetration of auxiliary flow 1 (AF1), and, as a result, for case B with the higher Re the main flow occupies most of the micro lens and decreases the curvatures. Furthermore, because of different flow rates of AF1 on the top and bottom, both cases show asymmetry in the top and bottom interfaces. The shape of each two-phase regions (red contours in Fig. 3) which is confined by the core flow on one side and AF2 on the other

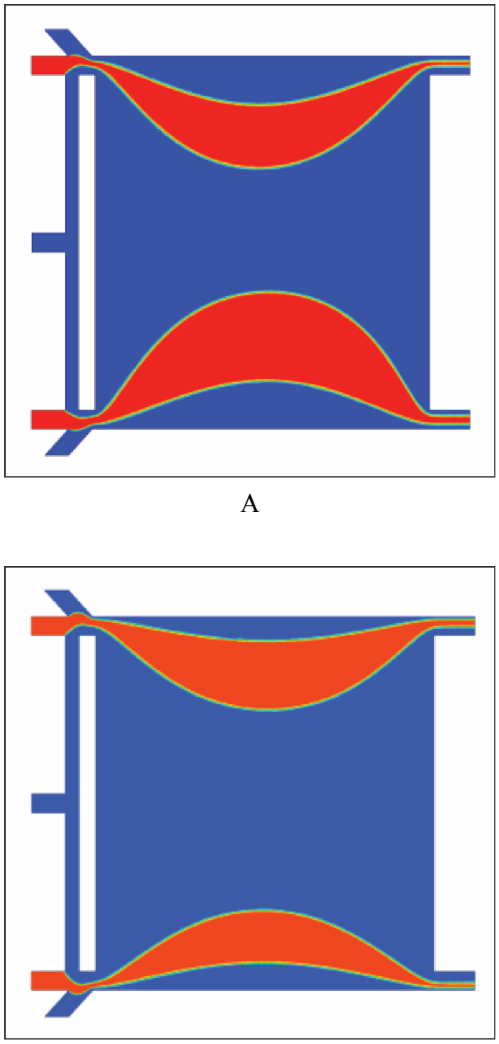

Fig. 3. Volume fraction of AF1 for case A and B

side, is affected by the volume flow rate of AF1. For case A that has smaller flow rate of AF1 in top, compared to bottom (q_2* = Q_2/Q_1 = 0.6), the fluidic lens in bottom penetrates further in the domain with higher curvature while for case B with (q_2* = Q_2/Q_1 = 2.0) the situation is reversed and the top region has higher curvature.

3.2 Ray tracking

Fig. 4 shows ray tracking for the simulations shown

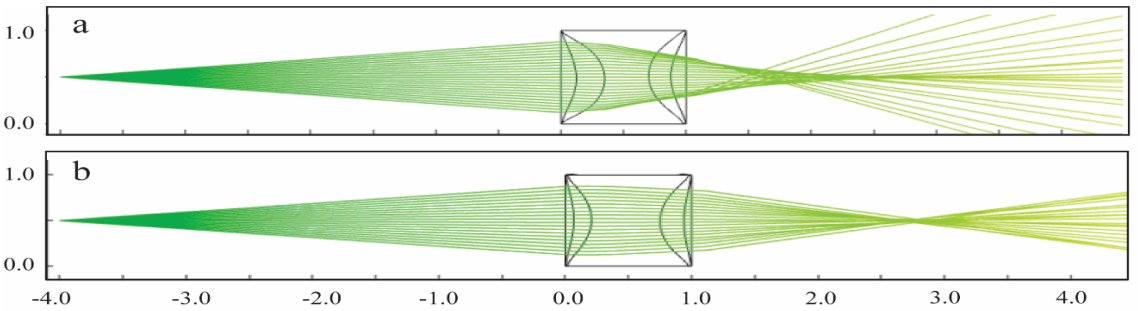

Fig. 4. Ray traces for micro lens corresponds to a) case A (Fig. 3(a)) and b) case B (Fig. 3(b))

in Fig. 3. For the ray tracking, the location of the interface estimated as the location of volume fraction ϕ = 0.5 for AF1, and data exported to the COMSOL Multiphysics software where the ray tracking is performed via optic module. It is evident from Fig. 4 that, for the higher curvature, the entrance side of ray results in a diffused focal point and the rays does not converge to a single point (Fig. 4(a)). On the other hand, for case B, simulation of ray tracking shows a single focal point of 1.75 mm from the right side of the lens.

3.3 Volume flow rate and focal point relation

Using the results from all simulations and with the JMP software, the final regression is performed on the data to obtain the relation between volume flow rate and focal point of micro-lens. It is notable that, in the regression process, the cases similar to case A (Fig. 4(a)) which does not have a sharp focal point are ignored and only the data related to the sharp points are considered for the regression. The final relation is given below:

where L is the focal point in mm and the coefficients α, β, ɣ, and η are given in Table 2 for case A and case B.

Table 2. Coefficients of Eq. 6 for case A and B

	α	β	γ	η
Case A	2.91	0.22	-0.12	-0.06
Case B	2.96	0.13	-0.09	-0.08

$$L=\alpha+\beta\left(\frac{q_0^*-8.25}{6.75}\right)+\gamma\left(\frac{q_2^*-1.25}{0.75}\right)+\eta\left(\frac{\mathrm{Re}-15.5}{14.5}\right) \quad (6)$$

4. Conclusions

Numerical simulations of three-fluid optofluidic micro-lens are performed using ANSYS Fluent software. Various conditions and flow rates are considered for each flow stream to compute the fluids interfaces inside the micro lens. These interfaces act like a lens and can be used to manipulate optic rays. The computed interfaces are exported to COMSOL Multiphysics software where a ray tracking simulation is performed for each lens. The number of simulations and their corresponding properties are determined via space filling design of experiment using the JMP software. A multivariable regression is performed with JMP to find a relation between the focal point of the micro lens and the volume flow rates of incoming flows to the micro lens.

References

1) Li, H., Song, C., Luong, T.D., Nguyen, N.T. and Wong, T.N., 2012. "An electrokinetically tunable optofluidic bi-concave lens", *Lab on a Chip*, vol.12, no.19, pp.3680-3687.
2) Nguyen, N.T., 2010. "Micro-optofluidic lenses: a review", *Biomicrofluidics*, vol.4, no.3, p.031501.
3) Song, C., Nguyen, N.T., Yap, Y.F., Luong, T.D.

and Asundi, A.K., 2011. “Multi-functional, optofluidic, in-plane, bi-concave lens: tuning light beam from focused to divergent”, *Microfluidics and nanofluidics*, vol.10, no.3, pp.671-678.

4) Rosenauer, M. and Vellekoop, M.J., 2009. “3D fluidic lens shaping–a multiconvex hydrodynamically adjustable optofluidic microlens”, *Lab on a Chip*, vol.9, no.8, pp.1040-1042.

5) Mao, X., Stratton, Z.I., Nawaz, A.A., Lin, S.C.S. and Huang, T.J., 2010. “Optofluidic tunable microlens by manipulating the liquid meniscus using a flared microfluidic structure”, *Biomicrofluidics*, vol.4, no.4, p.043007.

6) Dong, L. and Jiang, H., 2006. “p H-adaptive microlenses using pinned liquid-liquid interfaces actuated by p H-responsive hydrogel”, *Applied physics letters*, vol.89, no.23, p.211120.

7) Dong, L., Agarwal, A.K., Beebe, D.J. and Jiang, H., 2007. “Variable-focus liquid microlenses and microlens arrays actuated by thermoresponsive hydrogels”, *Advanced Materials*, vol.19, no.3, pp.401-405.

8) Tang, S.K., Stan, C.A. and Whitesides, G.M., 2008. “Dynamically reconfigurable liquid-core liquid-cladding lens in a microfluidic channel”, *Lab on a Chip*, vol.8, no.3, pp.395-401.

9) Mao, X., Lin, S.C.S., Lapsley, M.I., Shi, J., Juluri, B.K. and Huang, T.J., 2009. “Tunable Liquid Gradient Refractive Index (L-GRIN) lens with two degrees of freedom”, *Lab on a Chip*, vol.*9*, no.14, pp.2050-2058.

10) Mao, X., Waldeisen, J.R., Juluri, B.K. and Huang, T.J., 2007. “Hydrodynamically tunable optofluidic cylindrical microlens”, *Lab on a Chip*, vol.7, no.10, pp.1303-1308.

11) Dong, L. and Jiang, H., 2008. “Selective formation and removal of liquid microlenses at predetermined locations within microfluidics through pneumatic control”, *Journal of Microelectromechanical Systems*, vol.17, no.2, pp.381-392.

12) Chen, Q., Li, T., Li, Z., Long, J. and Zhang, X., 2018. “Optofluidic tunable lenses for in-plane light manipulation”, *Micromachines*, vol.9, no.3, p.97..

13) Li, L., Wang, J.H., Wang, Q.H. and Wu, S.T., 2018. “Displaceable and focus-tunable electrowetting optofluidic lens”, *Optics express*, vol.26, no.6, pp.25839-25848.

14) Mishra, K. and Mugele, F., 2016. “Numerical analysis of electrically tunable aspherical optofluidic lenses”, *Optics express*, vol 24, no.13, pp. 14672-14681.

15) Lima, N.C., Mishra, K. and Mugele, F., 2017. “Aberration control in adaptive optics: a numerical study of arbitrarily deformable liquid lenses”, *Optics express*, vol25, no.6, pp.6700-6711.

16) The Ray Optics Module User’s guide, COMSOL Multiphysics